STROKE

Brain-released alarmins and stress response synergize in accelerating atherosclerosis progression after stroke

Stefan Roth,[1,2] Vikramjeet Singh,[1,2] Steffen Tiedt,[1,2] Lisa Schindler,[1,2] Georg Huber,[3] Arie Geerlof,[3] Daniel J. Antoine,[4] Antoine Anfray,[5] Cyrille Orset,[5] Maxime Gauberti,[5] Antoine Fournier,[5] Lesca M. Holdt,[6] Helena Erlandsson Harris,[7] Britta Engelhardt,[8] Marco E. Bianchi,[9] Denis Vivien,[5] Christof Haffner,[1] Jürgen Bernhagen,[1,2] Martin Dichgans,[1,2] Arthur Liesz[1,2]*

Stroke induces a multiphasic systemic immune response, but the consequences of this response on atherosclerosis—a major source of recurrent vascular events—have not been thoroughly investigated. We show that stroke exacerbates atheroprogression via alarmin-mediated propagation of vascular inflammation. The prototypic brain-released alarmin high-mobility group box 1 protein induced monocyte and endothelial activation via the receptor for advanced glycation end products (RAGE)–signaling cascade and increased plaque load and vulnerability. Recruitment of activated monocytes via the CC-chemokine ligand 2–CC-chemokine receptor type 2 pathway was critical in stroke-induced vascular inflammation. Neutralization of circulating alarmins or knockdown of RAGE attenuated atheroprogression. Blockage of β3-adrenoreceptors attenuated the egress of myeloid monocytes after stroke, whereas neutralization of circulating alarmins was required to reduce systemic monocyte activation and aortic invasion. Our findings identify a synergistic effect of the sympathetic stress response and alarmin-driven inflammation via RAGE as a critical mechanism of exacerbated atheroprogression after stroke.

INTRODUCTION

The risk of recurrent vascular events after stroke is high and remains elevated even years after first stroke (*1*, *2*). The enhanced risk of secondary events encompasses large artery stroke and myocardial infarction, both manifestations of atherosclerosis (*3*, *4*). Atherosclerosis is a chronic inflammatory condition of the arterial vessel wall, characterized by an imbalance in lipid metabolism and recruitment of immune cells leading to a chronic inflammatory milieu (*5*, *6*). Key steps further include infiltration by monocytes, secretion of proteolytic enzymes, fibrous cap thinning, and plaque rupture, eventually causing end-organ damage due to ischemia. Previous work in experimental myocardial infarction has demonstrated an accelerating effect of this event on atheroprogression (*7*, *8*), which has recently been linked to a stress-mediated mobilization of monocytes from bone marrow niches via adrenergic signaling (*7*). The same study further provided initial evidence for accelerated atheroprogression after experimental stroke (*7*). However, the mechanisms underlying enhanced atheroprogression after stroke have so far not been investigated.

Stroke promotes a multiphasic immunomodulation in the systemic immune compartment with an early sterile inflammatory response within hours and a chronic inflammatory response that is observed both in mice and in stroke patients (*9*–*11*). We previously demonstrated that this systemic immunomodulation is triggered by alarmins released from necrotic brain tissue (*12*). This specifically involves the prototypic alarmin high-mobility group box 1 (HMGB1). Alarmins can have chemoattractant as well as cytokine-inducing properties and interact with pattern recognition receptors such as toll-like receptors and the receptor for advanced glycation end products (RAGE) on various immune and nonimmune cell populations (*13*).

In light of these observations, we hypothesized that stroke might promote vascular inflammation and atheroprogression via an alarmin-driven systemic immune response. Here, we confirm exacerbation of atheroprogression after stroke and specifically identify a key role of the alarmin-RAGE pathway acting in synergy with the sympathetic stress response for de novo recruitment of activated monocytes to atherosclerotic lesions.

RESULTS

Stroke exacerbates atheroprogression via increased vascular monocyte recruitment

To determine the effect of stroke on exacerbation of atheroprogression, we fed 8-week-old apolipoprotein E–deficient (*ApoE*$^{-/-}$) mice (*14*), a well-established mouse model for atherosclerosis, a high-cholesterol diet (HCD) for 8 weeks before the induction of experimental stroke and assessed plaque load after an additional 4 weeks of HCD (Fig. 1A and fig. S1). Overall plaque load in whole aorta was significantly ($P = 0.002$) increased in mice undergoing stroke surgery compared to sham surgery as assessed by en face staining (Fig. 1B). Likewise, significantly ($P < 0.0001$) increased plaque load was observed throughout the aortic valve (Fig. 1, C to E). Similar results were also obtained in female animals (fig. S2). To evaluate whether stroke-induced plaque formation was accompanied by vascular inflammation, we next performed flow cytometric analysis of whole-aorta cell suspensions. In contrast to other immune cell populations (fig. S3), monocyte cell counts and, more specifically, the number of proinflammatory CD11b^{+} Ly6C^{high} monocytes per aorta were increased after stroke compared to sham (Fig. 1, F and G). We further found an increase in the enzymatic

[1]Institute for Stroke and Dementia Research, Klinikum der Universität München, 81377 Munich, Germany. [2]Munich Cluster for System Neurology (SyNergy), 80336 Munich, Germany. [3]Institute of Structural Biology, Helmholtz Centre Munich, 85764 Munich, Germany. [4]Medical Research Council Center for Drug Safety Science, Department for Molecular and Clinical Pharmacology, University of Liverpool, L69 3GE Liverpool, UK. [5]INSERM, Université de Caen-Normandie, CHU de Caen, INSERM UMR-S U1237, Physiopathology and Imaging of Neurological Disorders, GIP Cyceron, 14074 Caen, France. [6]Institute of Laboratory Medicine, Klinikum der Universität München, 81377 Munich, Germany. [7]Department of Medicine, Karolinska University Hospital, SE-171 76 Stockholm, Sweden. [8]Theodor Kocher Institute, University of Bern, Freiestrasse 1, 3012 Bern, Switzerland. [9]Faculty of Medicine, San Raffaele University, 20132, Milan, Italy.
*Corresponding author. Email: arthur.liesz@med.uni-muenchen.de

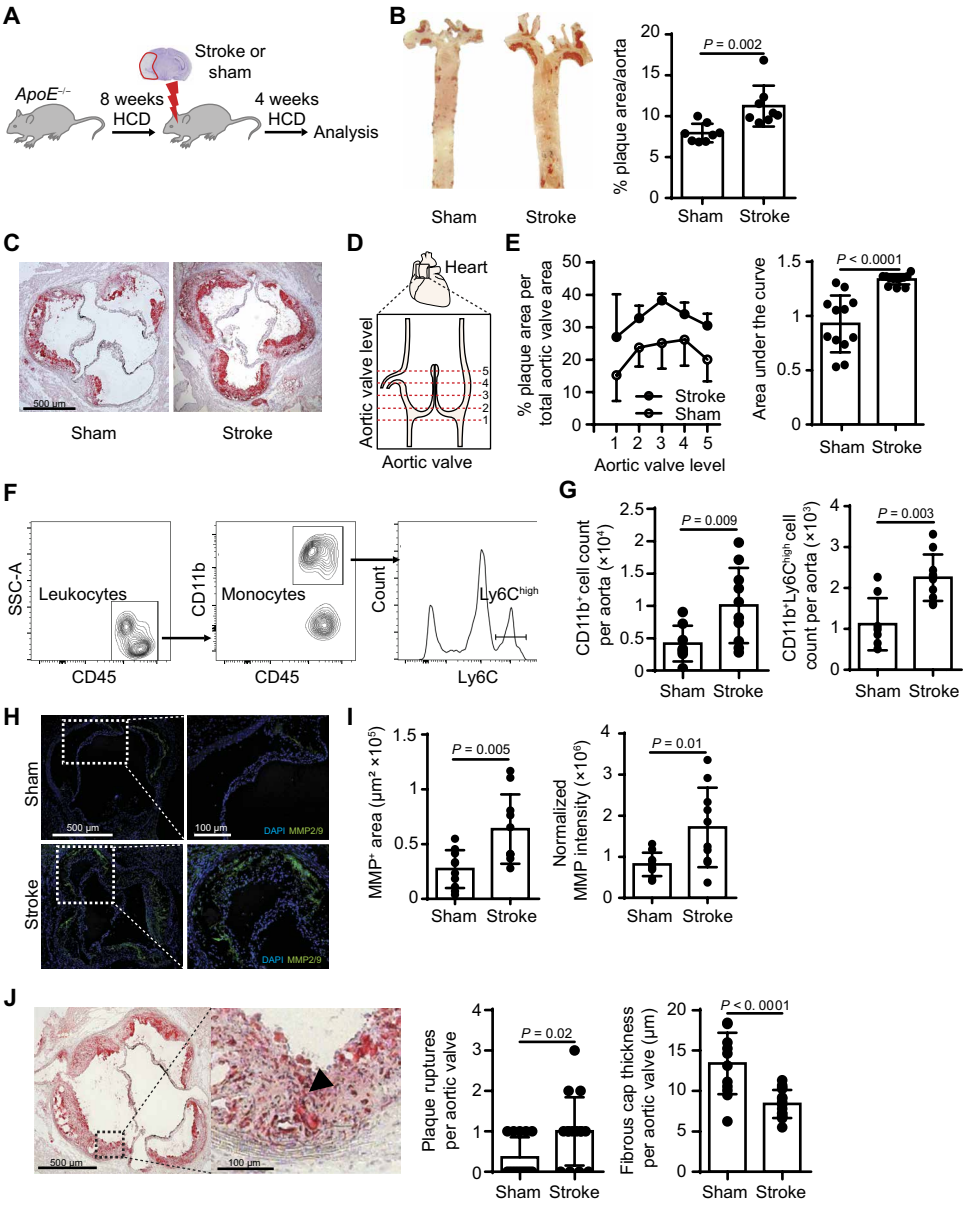

Fig. 1. Stroke exacerbates atheroprogression. (**A**) Experimental design: Apolipoprotein E–deficient mice fed a high-cholesterol diet (HCD-fed *ApoE*$^{-/-}$) underwent stroke or sham surgery and were sacrificed 1 month after surgical procedure. (**B**) Representative whole-aorta en face Oil Red O staining in sham and stroked mice (left) and quantification of the plaque load 1 month after stroke in sham and stroked animals (right, *U* test, $n = 8$ per group). (**C**) Representative images of Oil Red O–stained aortic valve sections 1 month after stroke or sham surgery. (**D**) Schematic representation of aortic valve. Red lines indicate the location of the sections analyzed in the study. (**E**) Quantification of aortic valve plaque load shown as percentage of plaque area per aortic valve in each section shown in (D) (left) and the area under the curve (right, *U* test, $n = 12$ per group). (**F**) Representative gating strategy for flow cytometric analysis of aortic monocytes. SSC-A, side scatter area. (**G**) Flow cytometric analysis of whole-aorta lysates showing total monocytes (CD11b^{+}; left) and the proinflammatory subset (Ly6C^{high}; right) cell counts after stroke induction compared to sham (*U* test, $n = 9$ to 10 per group). (**H**) Representative images of aortic valve in situ zymography for 4′,6-diamidino-2-phenylindole (DAPI) (nuclear marker, blue) and matrix metalloproteinase 2/9 (MMP2/9) (representing enzymatically active areas, green) 1 month after surgery. (**I**) Quantification of MMP2/9 activity shown as enzymatically active area and normalized intensity (*U* test, $n = 12$ per group). (**J**) Representative images of Oil Red O–stained aortic valve sections 1 month after stroke (left) and quantification of number of plaque ruptures and cap thickness in aortic valve sections 1 month after sham or stroke surgery (*U* test, $n = 14$ to 15 per group). The arrowhead in the high-magnification image indicates a buried fibrous cap in lesion.

activity of matrix metalloproteinase 2 (MMP2) and MMP9 as detected by in situ zymography (Fig. 1, H and I). Because increased MMP activity is associated with plaque instability (*15*), we further investigated morphological markers of vulnerable plaques using previously established protocols (*16*). Cap thickness was reduced, and the number of highly unstable plaques increased in mice undergoing stroke surgery compared to sham surgery, suggesting a more vulnerable plaque morphology after stroke (Fig. 1J). Moreover, we analyzed plaques at the carotid bifurcation area, a predilected site for stenosis and plaque rupture in stroke patients, observing also in this area a trend toward increased plaque load after stroke (fig. S4). To determine whether the increased vascular inflammation was due to local proliferation or de novo recruitment of proinflammatory monocytes, we next implanted osmotic pumps releasing bromdeoxyurdine (BrdU) for detection of cell proliferation. In addition, we intraperitoneally (ip) administered 1×10^7 CCR2$^{RFP/+}$ reporter monocytes, expressing red fluorescent protein (RFP) under the CC-chemokine receptor type 2 (CCR2) promoter, for detection of proinflammatory monocyte recruitment in HCD-fed *ApoE*$^{-/-}$ mice after stroke or sham surgery (Fig. 2A). Although we found no difference in the proliferation rate of aortic monocytes/macrophages as assessed by BrdU incorporation (Fig. 2B and fig. S5), the recruitment of ip injected proinflammatory CCR2$^{RFP/+}$ reporter cells into the aorta was substantially increased in stroke compared to sham group (Fig. 2, C and D, and fig. S6).

Stroke induces chemoattractant expression and endothelial activation

Next, we investigated the mechanisms underlying active aortic monocyte recruitment after stroke and explored the possibility that stroke treatment may elicit a specific chemokine/cytokine profile in the atherogenic aorta. To investigate the aortic chemokine profile, we performed a polymerase chain reaction (PCR) array for 86 chemokines and chemoattractant receptors using lysates of whole aortas obtained 3 days after stroke or sham surgery (table S1). We found that the transcription of 12 chemokines and chemoattractant receptors was up-regulated after stroke compared to sham (Fig. 2E). Notably, the

Fig. 2. Stroke increases vascular inflammation via recruitment of inflammatory monocytes to atherosclerotic plaques. (**A**) Schematic illustration of experimental design for data shown in (B) to (D): HCD-fed *ApoE*$^{-/-}$ mice underwent sham or stroke surgery and received either continuous bromdeoxyurdine (BrdU) administration or CCR2$^{RFP/+}$ bone marrow–derived cells intraperitoneally (ip). After 1 week, mice were sacrificed, and aortas and lymphoid organs were analyzed. (**B**) Analysis of BrdU^{+}CD11b^{+} monocytes from aortas after stroke or sham surgery (*U* test, $n = 5$ to 7 per group). (**C**) Gating strategy and representative histogram plots (right) for invading red fluorescent protein–positive (RFP^{+}) monocytes in aortas (white, sham; gray, stroke) and (**D**) corresponding quantification of RFP^{+}CD11b^{+} monocytes in aorta (*U* test, $n = 5$ to 6 per group). (**E**) Fold change (FC) and adjusted *P* values (in parentheses) of chemokine and chemokine receptor transcription in aorta lysates 3 days after stroke compared to sham surgery (left; $n = 3$ per group, $P < 0.1$) and corresponding volcano plot for transcriptional regulation determined by real-time polymerase chain reaction arrays (right panel; *x* axis = fold change; *y* axis = *P* value, cutoff at <0.1). (**F**) Serum levels of CC-chemokine ligand 2 (CCL2) 1 week after stroke compared to sham surgery (*U* test, $n = 4$ to 6 per group). (**G**) Flow cytometric analysis of aortic CCR2^{+}Ly6C^{high} monocytes (left) and CC-chemokine receptor type 2–positive (CCR2^{+}) surface expression on inflammatory Ly6C^{high} monocytes (right) in aortas 3 days after stroke or sham surgery (*U* test, $n = 7$ per group). (**H**) Quantification of aortic invasion of adoptively transferred RFP-reporter cells from either CCR2-deficient (CCR2$^{RFP/RFP}$) or CCR2^{+} RFP^{+} donor mice (CCR2$^{RFP/+}$) (*U* test, $n = 5$ to 6 per group).

most up-regulated chemokine was CC-chemokine ligand 2 (CCL2), with a more than sixfold increase after stroke induction (fold change, 6.316; $P = 0.018$). CCL2 is secreted by foam cells in arterial lesions (*17*) and by activated endothelium (*18*) and attracts proinflammatory CCR2-expressing cells (*19*–*21*). Hence, we analyzed serum of mice after stroke and found increased CCL2 concentrations compared to sham-operated mice 1 week after sham surgery (Fig. 2F). In addition, we measured monocytic CCR2 expression by flow cytometry in aortas after stroke versus sham surgery, and we observed an increase in CCR2^{+} cell counts as well as CCR2 surface expression on inflammatory monocytes (Fig. 2G). One week after stroke induction, we detected fewer CD11b^{+}Ly6C^{high} RFP^{+} monocytes in the aortas of mice injected ip with homozygous CCR2$^{RFP/RFP}$ (CCR2-deficient) compared to heterozygous CCR2$^{RFP/+}$ (CCR2-expressing) cells after stroke induction (Fig. 2H), indicating a critical role of the CCL2-CCR2 pathway in attraction of proinflammatory monocytes to the aorta after stroke.

Atherogenic monocyte recruitment is mediated by an orchestrated interplay of chemokine/chemokine receptor and integrin/adhesion molecule interactions with a pivotal role for endothelial activation. We found an increase mRNA expression of *Icam1* and *Vcam1*, key adhesion molecules in atherogenic monocyte recruitment, in aortas 3 days after stroke (Fig. 3A). In vivo molecular magnetic resonance imaging (MRI) using microsized particles of iron oxide–labeled vascular cell

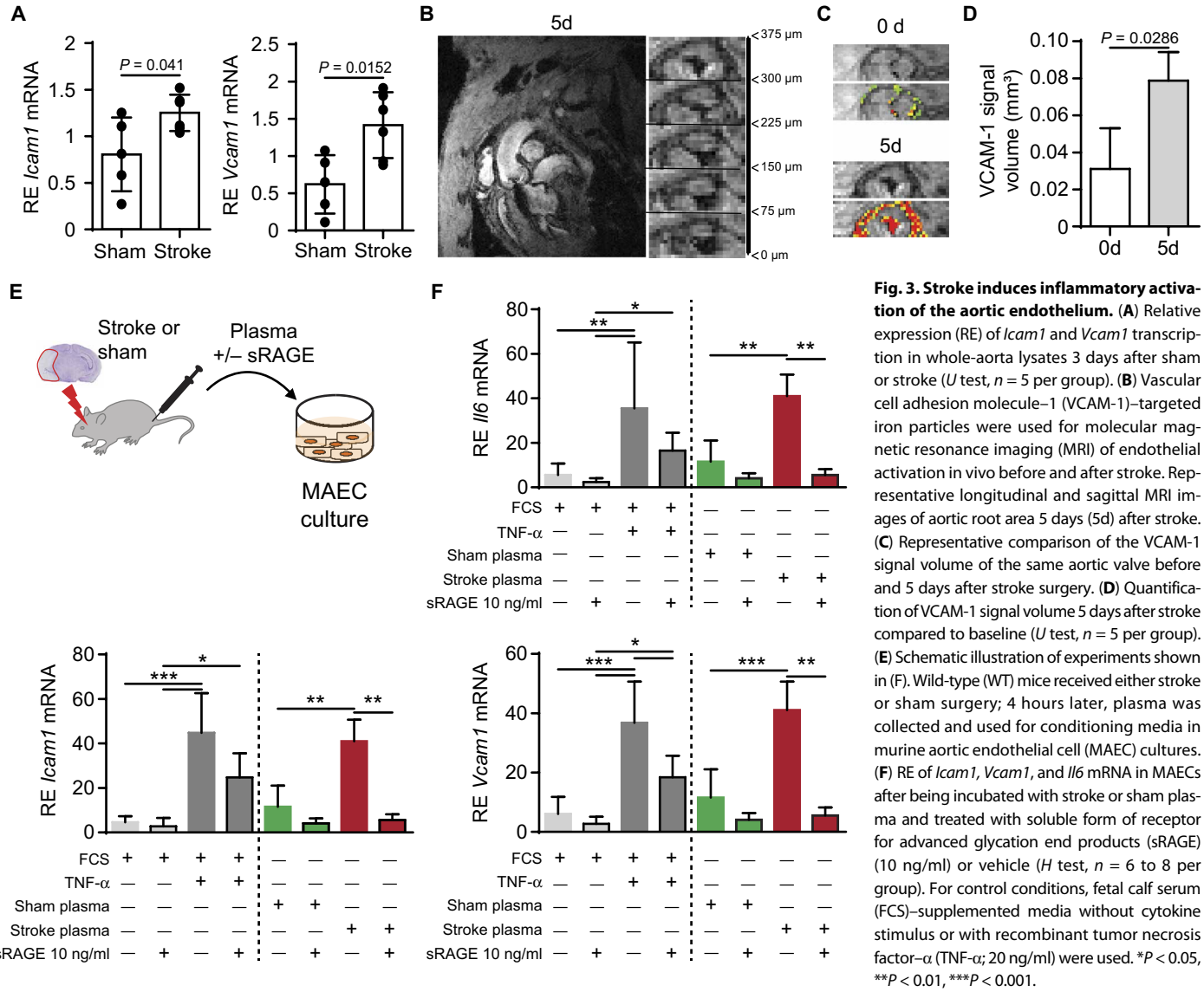

Fig. 3. Stroke induces inflammatory activation of the aortic endothelium. (**A**) Relative expression (RE) of *Icam1* and *Vcam1* transcription in whole-aorta lysates 3 days after sham or stroke (*U* test, $n = 5$ per group). (**B**) Vascular cell adhesion molecule–1 (VCAM-1)–targeted iron particles were used for molecular magnetic resonance imaging (MRI) of endothelial activation in vivo before and after stroke. Representative longitudinal and sagittal MRI images of aortic root area 5 days (5d) after stroke. (**C**) Representative comparison of the VCAM-1 signal volume of the same aortic valve before and 5 days after stroke surgery. (**D**) Quantification of VCAM-1 signal volume 5 days after stroke compared to baseline (*U* test, $n = 5$ per group). (**E**) Schematic illustration of experiments shown in (F). Wild-type (WT) mice received either stroke or sham surgery; 4 hours later, plasma was collected and used for conditioning media in murine aortic endothelial cell (MAEC) cultures. (**F**) RE of *Icam1*, *Vcam1*, and *Il6* mRNA in MAECs after being incubated with stroke or sham plasma and treated with soluble form of receptor for advanced glycation end products (sRAGE) (10 ng/ml) or vehicle (*H* test, $n = 6$ to 8 per group). For control conditions, fetal calf serum (FCS)–supplemented media without cytokine stimulus or with recombinant tumor necrosis factor–α (TNF-α; 20 ng/ml) were used. $^{*}P < 0.05$, $^{**}P < 0.01$, $^{***}P < 0.001$.

adhesion molecule–1 (VCAM-1)–specific antibodies (*22*) revealed an increase in VCAM-1 signal volume at 5 days after stroke in aortic valves compared to baseline values before stroke induction (Fig. 3, B to D). These experiments provided strong support for the activation of the aortic endothelium after stroke. We hypothesized that the observed endothelial activation was likely mediated by soluble, proinflammatory mediators released from the ischemic brain as previously described by our group (*12*). To test this hypothesis, we used an in vitro endothelial culture system, subjecting murine aortic endothelial cells (MAECs) to stroke- or sham-conditioned plasma; control conditions included normal fetal calf serum–supplemented media with or without tumor necrosis factor–α (TNF-α) stimulation (Fig. 3E). We found that mRNA expression of *Vcam1*, *Icam1*, and *Il6* increased after conditioning with stroke plasma compared to sham plasma, with expression similar to stimulation of MAECs by TNF-α (Fig. 3F). Moreover, we found that addition of the soluble form of RAGE (sRAGE; 10 ng/ml) decreased the expression of *Vcam1*, *Icam1*, and *Il6* after stimulating the MAECs with stroke plasma. These results support the concept of poststroke endothelial activation by soluble plasma mediators such as cytokines and alarmins—druggable by decoy receptors such as sRAGE—with an ensuing active recruitment of monocytes via CCR2-dependent pathways.

Poststroke alarmin release induces immune activation via the RAGE signaling pathway

Acute stroke leads to massive release of proinflammatory alarmins such as the prototypic alarmin HMGB1 from hypoxia-stressed and necrotic tissue (*12*). We confirmed the increase of plasma HMGB1 concentrations acutely (24 hours) after experimental stroke and expanded this observation to the chronic phase (30 days) when HMGB1 plasma levels were still more than threefold elevated after stroke compared to sham (Fig. 4A). We next reduced systemic alarmins in vivo using sRAGE as a decoy receptor for circulating alarmins (*23*). We treated mice 30 min before surgery and 4 hours after surgery with an intraperitoneal bolus (4 mg/kg) of sRAGE or vehicle and compared monocytic activation and cytokine expression in whole-spleen

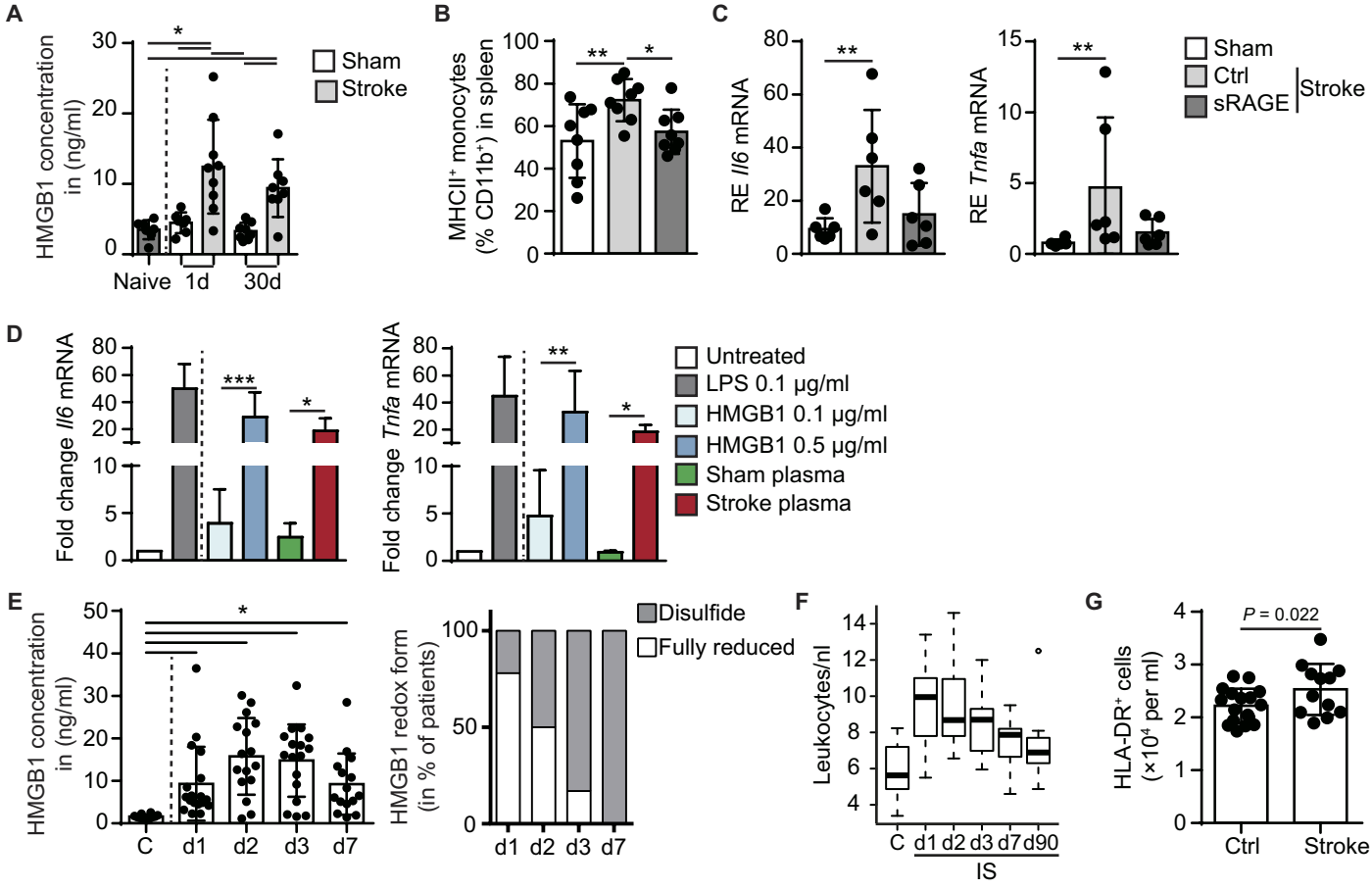

Fig. 4. HMGB1 induces systemic innate immune activation after stroke. (**A**) Plasma high-mobility group box 1 (HMGB1) concentrations were measured by enzyme-linked immunosorbent assay in naïve, sham, and stroke HCD-fed *ApoE*$^{-/-}$ mice 1 and 30 days after surgery [one-way analysis of variance (ANOVA), $n = 7$ to 9 per group). (**B**) Flow cytometric analysis of major histocompatibility complex class II–positive (MHCII$^+$) expression of splenic myeloid cells from HCD-fed *ApoE*$^{-/-}$ mice 3 days after stroke with vehicle or sRAGE treatment (one-way ANOVA, $n = 8$ per group). (**C**) RE of *Il6* and *Tnfa* mRNA in spleen of sham-operated and stroked vehicle-treated or sRAGE-treated WT mice 3 days after surgical procedure (*H* test, $n = 6$ per group). (**D**) RE of *Il6* and *Tnfa* mRNA of isolated murine splenic monocytes from WT mice, which were stimulated with recombinant HMGB1 (0.1 and 0.5 µg/ml), murine sham and stroke plasma (50%), and lipopolysaccharide (LPS) (0.1 µg/ml) in vitro (*H* test, $n = 5$ to 8 per group). (**E**) Plasma concentration of HMGB1 acquired by quantitative mass spectrometry analysis at different time points (days 1 to 7) in stroke patients and age-matched controls (C; left; $n = 15$ to 18 per group, one-way ANOVA). Changes in the distribution of HMGB1 reduction/oxidation (redox) state from fully reduced to disulfide state over the first week after stroke (right; $n = 15$ to 18 per group). (**F**) Quantification of blood leukocyte counts in ischemic stroke (IS) and control patients ($n = 15$ to 18 per group). (**G**) Flow cytometric analysis of human patient blood samples for human leukocyte antigen (HLA-DR$^+$) cell count as an indication of monocyte activation at up to 60 days after large IS compared to age-matched controls (*t* test, $n = 12$ to 17 per group). *$P < 0.05$, **$P < 0.01$, ***$P < 0.001$.

lysates 3 days after stroke. Compared to sham-operated mice, mice undergoing stroke surgery showed an increase of major histocompatibility complex class II (MHCII) expression as a monocytic activation marker (Fig. 4B) and elevated *Il6* and *Tnfa* mRNA expression (Fig. 4C). In contrast, sRAGE treatment abrogated the increase in MHCII expression and cytokine mRNA expression after stroke (Fig. 4, B and C). To investigate the role of soluble plasma mediators in monocyte activation more specifically, we treated primary monocyte cultures with recombinant HMGB1 or conditioned medium with plasma from sham-operated or stroked mice. Analysis of the mRNA expression revealed a dose-dependent increase in *Il6* and *Tnfa* expression after treatment with recombinant endotoxin-free HMGB1 as well as plasma from stroked animals, confirming a key role for soluble mediators such as HMGB1 in the activation of monocytes (Fig. 4D). Accordingly, we also detected substantially increased serum HMGB1 concentrations in human stroke patients both in the acute (within first 48 hours) and subacute phase (72 hours and 7 days) (Fig. 4E and table S2). Analysis of the different human HMGB1 reduction/oxidation (redox) forms by mass spectroscopy identified the functionally relevant cytokine-inducing disulfide HMGB1 isoform as the predominant modification after 3 days after stroke (Fig. 4E). This finding is in accordance with our previous observations on HMGB1 redox modifications in experimental stroke in mice showing that disulfide HMGB1 is the key mediator resulting in activation and expansion of the systemic monocyte population after stroke (*12*, *24*, *25*). The increase of proinflammatory HMGB1 was reflected in the pattern of transient leukocytosis during the time course after stroke (Fig. 4F). Moreover, C-reactive protein blood levels and neutrophil counts were increased after stroke, reflecting the alarmin-driven sterile inflammatory response (fig. S7). Accordingly, we also detected an increase in the frequency of activated human leukocyte antigen (HLA-DR$^+$) cells 2 months after human stroke (Fig. 4G).

In light of the effective abrogation of the poststroke systemic immune response in the presence of sRAGE, we aimed to test the effect of sRAGE treatment on stroke-induced atheroprogression. Atherosclerotic animals were treated before and after surgery with an intraperitoneal bolus (4 mg/kg) of sRAGE, and aortic plaque load was analyzed after sham or stroke surgery (Fig. 5A). We found reduced plaque loads in aortas of mice receiving sRAGE compared to control-treated mice after stroke, whereas no difference was detected for the sham-operated groups between control and sRAGE treatment (Fig. 5B). Correspondingly, the overall survival rate and normalization of poststroke weight loss were improved in sRAGE-treated animals (fig. S8), and the same pattern of treatment efficacy was observed for the plaque load in aortic valves (fig. S9). In addition, flow cytometric analysis revealed that sRAGE abrogated poststroke increase in total $CD45^+$ $CD11b^+$ as well as $CD11b^+Ly6C^{high}$ proinflammatory monocyte cell counts in aortas 4 weeks after stroke induction (Fig. 5C). Assessment of the lipid profiles of HCD-fed $ApoE^{-/-}$ mice revealed no differences after stroke induction and sRAGE treatment, except for the nonatherogenic (*26*) triglyceride levels (fig. S10).

Given the potent effect of sRAGE on neutralizing the effects of poststroke alarmins on vascular inflammation and atheroprogression, we aimed to more specifically investigate the contribution of the RAGE-dependent pathway. To down-regulate RAGE in vivo, we administered RAGE-specific small interfering RNA (siRNA) in HCD-fed $ApoE^{-/-}$ mice and found a knockdown of aortic *RAGE* mRNA and protein expression 3 days after hydrodynamic intravenous siRNA injection of 10 nmol of RAGE-silencing or negative control siRNA (Fig. 5, D and E). siRNA-induced *RAGE* knockdown reduced aortic total and proinflammatory monocyte counts 7 days after stroke induction compared to control treatment with unspecific siRNA (Fig. 5F). As RAGE also engages ligands other than HMGB1, we next aimed to test the specific contribution of HMGB1 as a potential mediator leading to RAGE-mediated atheroprogression. Neutralizing circulating HMGB1 by intraperitoneal injection of HMGB1-specific monoclonal antibodies (4 mg/kg) immediately after experimental ischemia attenuated the increase in cellular vascular inflammation after stroke induction (Fig. 5G). However, neither infarct volume nor behavioral deficits were affected by the sRAGE or HMGB1-specific antibody treatment compared to control treatment 1 week after experimental stroke. Moreover, using HMGB1-specific antibodies in wild-type (WT) mice reduced monocyte expansion and activation in blood and increased cell number in spleen 24 hours after stroke (fig. S11). To further elaborate on the role of HMGB1 as a proinflammatory mediator of atheroprogression, we administered recombinant HMGB1 to HCD-fed $ApoE^{-/-}$ mice without any surgical intervention. We found increased monocyte counts in whole-aorta lysates (Fig. 5H) and exacerbated plaque loads in aortic valves 7 days after HMGB1 injection (Fig. 5, I and J). In addition, we detected an up-regulation of *Il6*, *Icam1*, and *Vcam1* mRNA expression in whole-aorta lysates (fig. S12), resembling the proinflammatory expression pattern found in aortas of mice undergoing stroke (compared to Fig. 3A). Together, these results indicate that HMGB1—and potentially other alarmins released from the necrotic brain tissue—induces a sterile, systemic immune response via vascular RAGE, which in turn results in exacerbation of vascular inflammation after stroke.

Alarmin release and sympathetic stress response synergize in poststroke atheroprogression

We aimed to further dissect the differential contribution of the sympathetic innervation versus alarmin-driven cascades on the observed effects of systemic immune activation and vascular inflammation after stroke. In accord with earlier findings (*27*), we observed a decrease in overall myeloid cell count of the femur bone marrow at 24 hours after stroke (Fig. 6A). This was associated with an increase in tyrosine hydroxylase expression along sympathetic fibers in the femur bone marrow (Fig. 6, B and C). These results indicated a potential release of monocytes from the bone marrow after sympathetic innervation due to a stroke-induced stress response. We and others previously observed a splenic expansion of myeloid cells after stroke induction (*12*, *28*). Hence, we tested the possibility of myeloid cell trafficking from the bone marrow to the spleen after stroke using an in vivo cell-tracking approach. After in vivo labeling of the bone marrow by quantum dot (Qdot) nanocrystals—nanometer-scaled fluorophores incorporated in the cytoplasm of living cells—we found an increased number of $Qdot^+$ monocytes in spleen after stroke compared to sham surgery (Fig. 6, D and E), whereas the $Qdot^+$ cell count in bone marrow decreased after stroke (fig. S13). To further investigate the contribution of the splenic immune compartment to poststroke vascular inflammation, we performed splenectomy versus sham surgery in HCD-fed $ApoE^{-/-}$ mice before stroke induction in both groups. Seven days after stroke, we found reduced aortic monocyte counts in splenectomized animals and a decreased plaque load in aortic valves compared to the nonsplenectomized but stroked control group (Fig. 6, F and G); however, splenectomy had no effect on infarct severity or bone marrow monocyte count (fig. S14). Together, these findings suggest a role for sympathetic innervation in mobilization of myeloid cells from the bone marrow niche as well as maturation/activation of monocytes in the splenic immune compartment, thus contributing to stroke-induced atheroprogression.

To further test this hypothesis, we analyzed the differential contribution of the alarmin signaling cascade and sympathetic innervation on monocyte cellularity and activation using sRAGE decoy receptors and the β3-adrenoreceptor inhibitor SR59230A (*7*, *29*). Blocking β3-adrenoreceptors but not sRAGE treatment suppressed the egress of $CD11b^+CD45^+$ monocytes from the bone marrow, whereas both treatment regimens increased overall spleen cellularity (Fig. 6, H and I). Notably, β3-adrenoreceptor blockage did not alter HMGB1 plasma concentrations after stroke (fig. S15). sRAGE treatment abrogated monocyte activation in the spleen after stroke, whereas adrenoreceptor blockage affected MHCII up-regulation only when applied in combination with sRAGE (Fig. 6J). In blood, we observed similar treatment effects with only the combination of adrenoreceptor and sRAGE blockage being effective in decreasing monocyte activation (fig. S16). We further investigated synergistic effects of neutralizing sympathetic activation and alarmin neutralization on exacerbation of vascular inflammation after stroke. Although both treatments attenuated the increase in aortic monocyte counts after stroke, blocking of alarmin signaling using sRAGE was required to attenuate the increase in activated $MHCII^+$ monocytes in atherosclerotic lesions after stroke (Fig. 6K). We additionally analyzed the impact of adrenoreceptor and sRAGE blockage on aortic valve plaque load. In accordance with the synergistic effects of adrenoreceptor and sRAGE blockage on inflammatory markers of vascular inflammation, only the combined treatment was effective in reducing aortic plaque load compared to the control treatment (Fig. 6L). These results suggest that sympathetic activation during the acute stress response after stroke drives bone marrow egress of monocytic cells, whereas brain-released alarmins are required for monocyte activation (fig. S17).

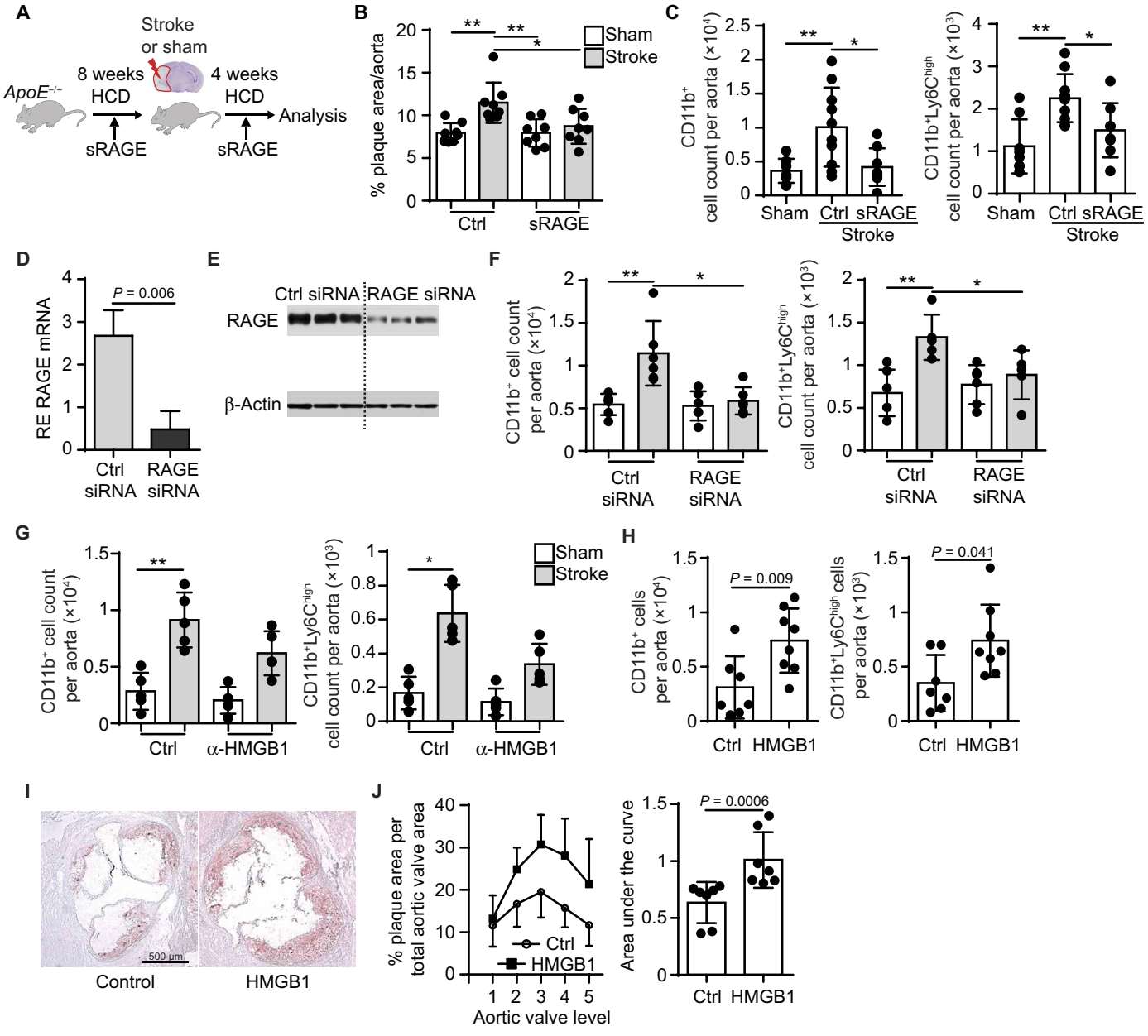

Fig. 5. Stroke induces atheroprogression via the RAGE-signaling pathway. (**A**) Schematic illustration of experimental design for data shown in (B) to (D): HCD-fed *ApoE*$^{-/-}$ mice received either an intraperitoneal injection of sRAGE or vehicle treatment 30 min before and 4 hours after the respective surgery and were sacrificed 1 month later. (**B**) Quantification of the overall plaque area per aorta 1 month after surgery in stroke or sham mice treated with sRAGE or vehicle (ANOVA, $n = 8$ per group). (**C**) Flow cytometric analysis of whole aorta for CD11b$^+$ and CD11b$^+$Ly6C^{high} monocyte counts after stroke with sRAGE or vehicle treatment compared to sham-operated mice 1 month after surgery (*H* test, $n = 7$ to 8 per group). (**D**) RAGE mRNA expression 3 days after hydrodynamic intravenous injection of RAGE-specific small interfering RNA (siRNA) or control siRNA (Ctrl; *U* test, $n = 5$ per group). (**E**) RAGE protein expression 3 days after RAGE-specific or control siRNA injection ($n = 3$ per group). (**F**) HCD-fed *ApoE*$^{-/-}$ mice received stroke or sham surgery 3 days after hydrodynamic RAGE-specific or control siRNA injection and were sacrificed 7 days later for flow cytometric analysis of whole aortas for CD11b$^+$ and CD11b$^+$Ly6C^{high} monocyte counts (*H* test, $n = 5$ to 6 per group). (**G**) Mice received HMGB1-specific or control immunoglobulin G antibodies immediately after surgery (sham or stroke), and CD11b$^+$ and CD11b$^+$Ly6C^{high} monocyte counts were analyzed with flow cytometry 7 days later (*H* test, $n = 5$ to 6 per group). (**H**) Flow cytometric analysis for CD11b$^+$ and CD11b$^+$Ly6C^{high} monocyte counts of whole aortas 7 days after an intraperitoneal injection of vehicle or rHMGB1 to HCD-fed *ApoE*$^{-/-}$ mice (*U* test, $n = 7$ to 8 per group). (**I**) Representative images of Oil Red O stained aortic valve sections 7 days after rHMGB1 administration. (**J**) Comparison of Oil Red O$^+$ area on five consecutive sections in aortic valves (left). Area under the curve analysis of the individual aortic valves (right) after HMGB1 administration compared to control-treated naïve *ApoE*$^{-/-}$ mice (*U* test, $n = 7$ per group). *$P < 0.05$, **$P < 0.01$.

DISCUSSION

Large-artery atherosclerosis is a major cause of stroke that is also associated with an unexpectedly high recurrence rate (*1*, *2*). We have shown that experimental stroke induces exacerbation of atheroprogression. Enhanced vascular inflammation after stroke depended on a synergistic effect of sympathetic recruitment of monocytes from the

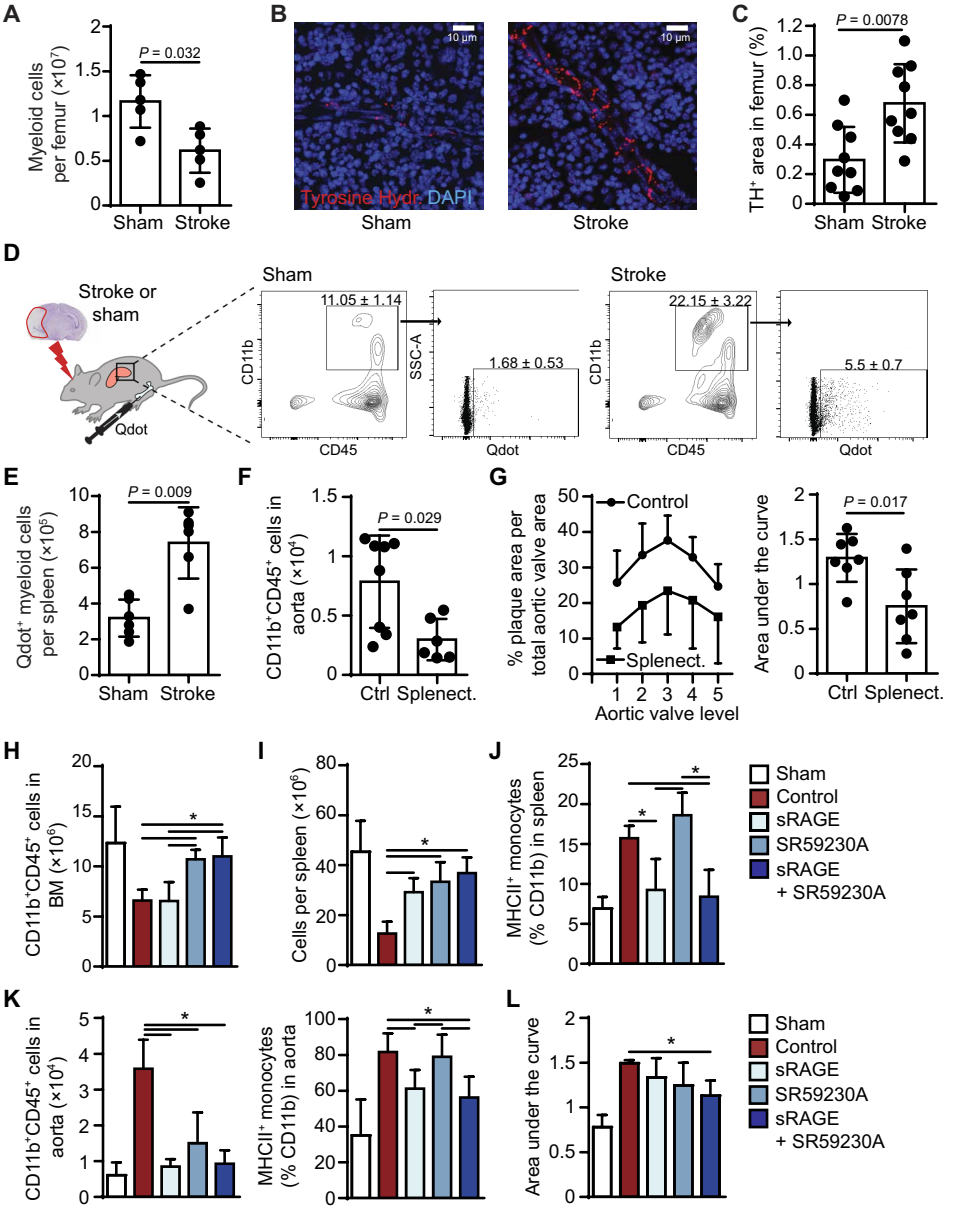

Fig. 6. Alarmin release and sympathetic stress response synergize in poststroke atheroprogression. (**A**) Flow cytometric analysis of myeloid cellularity in femur bone marrow 24 hours after stroke compared to sham surgery. (**B**) Representative images of immunofluorescence staining for tyrosine hydroxylase (TH) in femoral bone marrow 24 hours after stroke and sham surgery. (**C**) Quantification of TH^+ area after stroke compared to sham on femoral sections (*U* test, $n = 7$ per group). (**D**) WT mice received quantum dot (Qdot) nanocrystal injections in the femoral bone marrow 2 hours before stroke or sham surgery and were sacrificed 24 hours later (*U* test, $n = 6$ per group). Representative gating strategy for $CD45^+CD11b^+$ monocytes and $Qdot^+$ myeloid cells in spleen after stroke or sham surgery. (**E**) Quantification of total $Qdot^+$ myeloid cells in spleens after stroke compared to sham surgery (*U* test, $n = 5$ per group). (**F**) HCD-fed $ApoE^{-/-}$ mice were splenectomized (Splenect.) before stroke or sham surgery and analyzed 7 days after stroke for total monocyte cell counts and proinflammatory $Ly6C^{high}$ frequency in aortas 1 week after stroke. (**G**) Quantification of overall plaque area in aortic valves of splenectomized mice after stroke induction (*U* test, $n = 6$ to 8 per group). (**H** to **J**) WT mice received either sRAGE, β3-blocker SR59230, both combined, or vehicle treatment immediately after stroke, and bone marrow (BM) (H) and spleen (I and J) were analyzed by flow cytometry 24 hours later for the total myeloid ($CD45^+CD11b^+$) cell count and monocyte activation (percentage of $MHCII^+$ monocytes; *H* test, $n = 6$ to 8 per group). (**K**) HCD-fed $ApoE^{-/-}$ mice received sRAGE, SR59230, combination therapy, or control treatment immediately after stroke. Bar graphs represent the flow cytometric analysis of $CD45^+CD11b^+$ monocyte cell count, the percentage of $MHCII^+$ monocytes, and $Ly6C^{high}$ monocytes in aortas 1 week after stroke (*H* test, $n = 7$ to 8 per group). (**L**) Area under the curve analysis quantifying plaque load in five consecutive sections of aortic valve for HCD-fed $ApoE^{-/-}$ mice (*H* test, $n = 5$ to 6 per group). $^*P < 0.05$, $^{**}P < 0.01$.

bone marrow niche and subsequent activation of innate immune and endothelial cells by circulating alarmins, attracting inflammatory monocytes to atherosclerotic lesions. We further identified the HMGB1-RAGE pathway as a critical signaling mechanism eliciting the sterile inflammatory response after stroke.

We observed a rapid translocation of bone marrow monocytes to the spleen after stroke. Myeloid monocyte mobilization has previously been shown to be critically mediated by sympathetic signaling via β3-adrenoreceptors in myocardial infarction models (*27*). Accordingly, we showed an important role of β3-adrenoreceptors in stroke-induced monocyte mobilization using specific inhibitors. However, although blocking sympathetic innervation attenuated monocyte evasion from the bone marrow, it did not affect monocyte activation, vascular inflammation, or plaque growth. Notably, previous studies in experimental and clinical stroke have associated the sympathetic stress response with subacute immunosuppression but not monocyte activation or vascular inflammation (*30*). Hence, our results strengthen the concept of a second mechanism promoting the inflammatory response after stroke, independent of sympathetic activation.

Aside from eliciting a local immune response with microglial activation, the release of HMGB1 and other alarmins from necrotic brain tissue induces a systemic response with cellular activation and massive cytokine secretion in peripheral immune organs (*10*, *12*). Systemic immune activation involves a rapid sterile immune response acutely after stroke, followed by an immunosuppression during the subacute phase (days 2 to 7) after stroke. In addition, previous clinical studies have demonstrated a third phase characterized by a delayed chronic immune activation (from day 7 on) with elevated inflammatory markers for more than 1 year after stroke in patients (*9*, *31*). The biological activity of HMGB1 depends critically on its redox state (*32*, *33*). Fully reduced HMGB1 has chemoattractant properties, whereas disulfide HMGB1 has cytokine-inducing properties and the terminally oxidized sulfonyl HMGB1 is anti-inflammatory (*11*). We observed that HMGB1 levels in stroke patients not only remained substantially increased during the first week after stroke but that the

proinflammatory disulfide HMGB1 species became the predominant isoform over this time course.

Monocytes/macrophages play a critical role in the development and propagation of atherosclerotic lesions. Monocyte invasion into atherogenic lesions has been shown to be instrumental in the initiation of atherosclerosis. In this phase, the chemokine-ligand receptor interaction plays a pivotal role. Studies have shown that CCR2 expression on monocytes is essential for recruitment into the adventitial space and for further plaque development (*34*, *35*). In contrast, proliferation of macrophages has been demonstrated to be the key driver for lesion growth in established atherosclerosis (*36*). Surprisingly, we observed that poststroke exacerbation of established atherosclerotic lesions was associated with enhanced de novo recruitment of circulating monocytes to the vessel rather than increased local proliferation. A possible explanation for this phenomenon is that as a consequence of the strong inflammatory response after stroke, monocyte chemoattraction via the CCL2-CCR2 axis regains a predominant role for monocyte recruitment comparable to the initiation of the vascular inflammatory milieu (*37*). Aside from chemoattraction, endothelial expression of adhesion molecules is pivotal for monocyte recruitment. Intercellular adhesion molecule–1 (ICAM-1) and VCAM-1 are known to be essential for the arrest and extravasation of monocytes into the arterial wall (*38*). Our data unequivocally demonstrate the up-regulation of these critical adhesion molecules on aortic endothelial cells in mice by PCR, in vivo imaging, and in vitro cultures. In accord with our results, it was previously shown that HMGB1 can activate endothelial cells, leading to changes in the nuclear factors Sp-1 and nuclear factor κB, with subsequent up-regulation of adhesion molecules and proinflammatory cytokines (*18*).

We observed a highly consistent effect of poststroke exacerbation of atherosclerosis pathology both in female and male mice, in aortas and aortic valves, and verified this phenomenon by in vivo MRI. However, a limitation of this study is that we were not able to fully investigate the link between poststroke atheroprogression and enhanced plaque rupture as a cause of recurrent stroke in the mouse atherosclerosis model. Atherosclerotic lesions of aorta and large arteries in animal models, including the *ApoE*-deficient model used here, rarely develop spontaneous destabilization and rupture with occlusive vascular thrombosis. We observed several surrogate markers of increased plaque vulnerability; however, increased incidence of plaque rupture and secondary ischemic brain lesions will have to be tested in more specific models that mimic human plaque rupture and ultimately in prospective clinical studies.

In conclusion, our data identify stroke-induced alarmin release from the ischemic brain as a critical mechanism activating inflammatory pathways and acting in synergy with an acute stress response after stroke to exacerbate atherosclerosis. Interfering with this sterile immune response by neutralizing brain-released alarmins may provide a therapeutic approach for stroke patients.

MATERIAL AND METHODS

Study design

The goal of this study was to investigate atheroprogression after stroke and describe the underlying mechanisms in an experimental model of ischemic stroke in $ApoE^{-/-}$ mice. Sample sizes were calculated using GPower 3.1. On the basis of a previous report (*7*), we used a monocyte increase rate of 40% with an SD of 25%. Using an α error of 0.05 and power of 0.8, we calculated a group size of 8 (*t* test, two groups, unpaired).

Data were excluded from all mice that died during surgery. Detailed exclusion criteria for the experimental models were (i) insufficient middle cerebral artery (MCA) occlusion (blood flow reduction less than 80%), (ii) death during surgery, and (iii) lack of brain ischemia as quantified by histology (see table S3 for included/excluded animals per experiment). Animals were randomized to treatment groups, and all analyses were performed by investigators blinded to group allocation. Unblinding was performed after completion of statistical analysis. All animal experiments were performed and reported in accordance with the Animal Research: Reporting of In Vivo Experiments (ARRIVE) guidelines (*39*).

Experimental animals

All animal experiments were performed in accordance with the guidelines for the use of experimental animals and were approved by the government committee of Upper Bavaria (Regierungspraesidium Oberbayern, #175-2013). We used age-matched, male C57BL6/J mice (8 to 10 weeks, 22 to 24 g body weight; Charles River Laboratories). $ApoE^{-/-}$ (the Jackson Laboratory) mice were fed an HCD (#88137, ssniff). Transient filament occlusion was performed in all $ApoE^{-/-}$ after 8 weeks of HCD. CCR2-RFP knock-in mice were bred with CX3CR1–green fluorescent protein (GFP) mice (*40*).

Clinical stroke patient study population

Ischemic stroke patients were recruited within 24 hours of symptom onset. All patients had a final diagnosis of ischemic stroke as defined by an acute focal neurological deficit in combination with a diffusion-weighted imaging-positive lesion on MRI or a new lesion on a delayed computed tomography scan. Age- and comorbidity-matched patients without neurological disease were used as controls. The study was approved by the local ethics committee and was conducted in accordance with the Declaration of Helsinki and institutional guidelines. Written and informed consent was obtained from all subjects.

Statistical analysis

Data were analyzed using GraphPad Prism version 6.0. All summary data are expressed as means ± SD. All data sets were tested for normality using the Shapiro-Wilk normality test. The groups containing normally distributed data were tested using a two-way Student's *t* test (for two groups) or analysis of variance (ANOVA) (for more than two groups). The remaining data were analyzed using the Mann-Whitney *U* test (for two groups) or *H* test (for more than two groups). Similar variance was assured for all groups, which were statistically compared. Differences with a $P < 0.05$ were considered to be statistically significant. *P* values were adjusted for comparison of multiple comparisons using Bonferroni correction.

SUPPLEMENTARY MATERIALS

www.sciencetranslationalmedicine.org/cgi/content/full/10/432/eaao1313/DC1

Materials and Methods

Fig. S1. Characterization of the 60-min filament MCA occlusion (fMCAo) model.

Fig. S2. Exacerbation of atherosclerotic lesions in aortic valves of male and female HCD-fed $ApoE^{-/-}$ mice 1 month after fMCAo surgery.

Fig. S3. Immune cell counts in aorta of HCD-fed $ApoE^{-/-}$ mice 1 month after experimental stroke.

Fig. S4. Analysis of atherosclerotic plaque load at the common carotid artery bifurcation in HCD-fed $ApoE^{-/-}$ mice.

Fig. S5. Comparison of BrdU incorporation in aorta, blood, and spleen 1 week after experimental stroke surgery.

Fig. S6. $RFP^{+}CD11b^{+}$ cell counts in blood after experimental stroke surgery.

Fig. S7. Immunological data of stroke patients.

Fig. S8. Body weight and mortality in sRAGE treatment mice after stroke.
Fig. S9. Atherosclerotic lesions in aortic valves of male and female HCD-fed ApoE$^{-/-}$ mice 1 month after experimental stroke and sRAGE treatment.
Fig. S10. Lipid profile of plasma samples 1 month after experimental stroke surgery and sRAGE treatment.
Fig. S11. Flow cytometric analysis of spleen and blood 24 hours after experimental stroke with anti-HMGB1 treatment.
Fig. S12. Recombinant HMGB1 in vivo administration exacerbates atherosclerosis.
Fig. S13. Quantification of in vivo Qdot labeling of femoral bone marrow 24 hours after experimental stroke.
Fig. S14. Myeloid cell count in femoral bone marrow and brain infarct volumetry after splenectomy.
Fig. S15. Impact of β3-adrenoreceptor blockage on HMGB1 plasma levels after experimental stroke.
Fig. S16. Impact of β3-adrenoreceptor blockage (SR59230A), alarmin blockage (sRAGE), and combined treatment on blood immune cells in WT mice.
Fig. S17. Schematic overview of proposed mechanism of atheroprogression after stroke.
Table S1. Primer list for quantitative PCR array (mouse chemokines and receptors).
Table S2. Demographic and clinical characteristics of the study population.
Table S3. Number of (excluded/included) animals in accomplished experiments.
References (*41*–*49*)

REFERENCES AND NOTES

1. A. J. Grau, C. Weimar, F. Buggle, A. Heinrich, M. Goertler, S. Neumaier, J. Glahn, T. Brandt, W. Hacke, H.-C. Diener, Risk factors, outcome, and treatment in subtypes of ischemic stroke: The German stroke data bank. *Stroke* **32**, 2559–2566 (2001).
2. J. Putaala, E. Haapaniemi, A. J. Metso, T. M. Metso, V. Artto, M. Kaste, T. Tatlisumak, Recurrent ischemic events in young adults after first-ever ischemic stroke. *Ann. Neurol.* **68**, 661–671 (2010).
3. J. K. Lovett, A. J. Coull, P. M. Rothwell, Early risk of recurrence by subtype of ischemic stroke in population-based incidence studies. *Neurology* **62**, 569–573 (2004).
4. W. B. Kannel, P. Sorlie, P. M. Mcnamara, Prognosis after initial myocardial infarction: The Framingham study. *Am. J. Cardiol.* **44**, 53–59 (1979).
5. P. Libby, Inflammation in atherosclerosis. *Nature* **420**, 868–874 (2002).
6. C. Weber, H. Noels, Atherosclerosis: Current pathogenesis and therapeutic options. *Nat. Med.* **17**, 1410–1422 (2011).
7. P. Dutta, G. Courties, Y. Wei, F. Leuschner, R. Gorbatov, C. S. Robbins, Y. Iwamoto, B. Thompson, A. L. Carlson, T. Heidt, M. D. Majmudar, F. Lasitschka, M. Etzrodt, P. Waterman, M. T. Waring, A. T. Chicoine, A. M. van der Laan, H. W. M. Niessen, J. J. Piek, B. B. Rubin, J. Butany, J. R. Stone, H. A. Katus, S. A. Murphy, D. A. Morrow, M. S. Sabatine, C. Vinegoni, M. A. Moskowitz, M. J. Pittet, P. Libby, C. P. Lin, F. K. Swirski, R. Weissleder, M. Nahrendorf, Myocardial infarction accelerates atherosclerosis. *Nature* **487**, 325–329 (2012).
8. A. P. Wright, M. K. Öhman, T. Hayasaki, W. Luo, H. M. Russo, C. Guo, D. T. Eitzman, Atherosclerosis and leukocyte–endothelial adhesive interactions are increased following acute myocardial infarction in apolipoprotein E deficient mice. *Atherosclerosis* **212**, 414–417 (2010).
9. J. Schulze, D. Zierath, P. Tanzi, K. Cain, D. Shibata, A. Dressel, K. Becker, Severe stroke induces long-lasting alterations of high-mobility group box 1. *Stroke* **44**, 246–248 (2013).
10. H. Offner, S. Subramanian, S. M. Parker, M. E. Afentoulis, A. A. Vandenbark, P. D. Hurn, Experimental stroke induces massive, rapid activation of the peripheral immune system. *J. Cereb. Blood Flow Metab.* **26**, 654–665 (2006).
11. V. Singh, S. Roth, R. Veltkamp, A. Liesz, HMGB1 as a key mediator of immune mechanisms in ischemic stroke. *Antioxid. Redox Signal.* **24**, 635–651 (2016).
12. A. Liesz, A. Dalpke, E. Mracsko, D. J. Antoine, S. Roth, W. Zhou, H. Yang, S.-Y. Na, M. Akhisaroglu, T. Fleming, T. Eigenbrod, P. P. Nawroth, K. J. Tracey, R. Veltkamp, DAMP signaling is a key pathway inducing immune modulation after brain injury. *J. Neurosci.* **35**, 583–598 (2015).
13. J. Li, R. Kokkola, S. Tabibzadeh, R. Yang, M. Ochani, X. Qiang, H. E. Harris, C. J. Czura, H. Wang, L. Ulloa, H. Wang, H. S. Warren, L. L. Moldawer, M. P. Fink, U. Andersson, K. J. Tracey, H. Yang, Structural basis for the proinflammatory cytokine activity of high mobility group box 1. *Mol. Med.* **9**, 37–45 (2003).
14. A. S. Plump, J. D. Smith, T. Hayek, K. Aalto-Setälä, A. Walsh, J. G. Verstuyft, E. M. Rubin, J. L. Breslow, Severe hypercholesterolemia and atherosclerosis in apolipoprotein E-deficient mice created by homologous recombination in ES cells. *Cell* **71**, 343–353 (1992).
15. J. L. Johnson, A. H. Baker, K. Oka, L. Chan, A. C. Newby, C. L. Jackson, S. J. George, Suppression of atherosclerotic plaque progression and instability by tissue inhibitor of metalloproteinase-2: Involvement of macrophage migration and apoptosis. *Circulation* **113**, 2435–2444 (2006).
16. J. Johnson, K. Carson, H. Williams, S. Karanam, A. Newby, G. Angelini, S. George, C. Jackson, Plaque rupture after short periods of fat feeding in the apolipoprotein E-knockout mouse: Model characterization and effects of pravastatin treatment. *Circulation* **111**, 1422–1430 (2005).
17. K. J. Moore, F. J. Sheedy, E. A. Fisher, Macrophages in atherosclerosis: A dynamic balance. *Nat. Rev. Immunol.* **13**, 709–721 (2013).
18. C. Fiuza, M. Bustin, S. Talwar, M. Tropea, E. Gerstenberger, J. H. Shelhamer, A. F. Suffredini, Inflammation-promoting activity of HMGB1 on human microvascular endothelial cells. *Blood* **101**, 2652–2660 (2003).
19. C.-L. Tsou, W. Peters, Y. Si, S. Slaymaker, A. M. Aslanian, S. P. Weisberg, M. Mack, I. F. Charo, Critical roles for CCR2 and MCP-3 in monocyte mobilization from bone marrow and recruitment to inflammatory sites. *J. Clin. Invest.* **117**, 902–909 (2007).
20. C. Shi, E. G. Pamer, Monocyte recruitment during infection and inflammation. *Nat. Rev. Immunol.* **11**, 762–774 (2011).
21. P. Dutta, H. B. Sager, K. R. Stengel, K. Naxerova, G. Courties, B. Saez, L. Silberstein, T. Heidt, M. Sebas, Y. Sun, G. Wojtkiewicz, P. F. Feruglio, K. King, J. N. Baker, A. M. van der Laan, A. Borodovsky, K. Fitzgerald, M. Hulsmans, F. Hoyer, Y. Iwamoto, C. Vinegoni, D. Brown, M. Di Carli, P. Libby, S. W. Hiebert, D. T. Scadden, F. K. Swirski, R. Weissleder, M. Nahrendorf, Myocardial infarction activates CCR2^{+} hematopoietic stem and progenitor cells. *Cell Stem Cell* **16**, 477–487 (2015).
22. M. Gauberti, A. Montagne, O. A. Marcos-Contreras, A. Le Béhot, E. Maubert, D. Vivien, Ultra-sensitive molecular MRI of vascular cell adhesion molecule-1 reveals a dynamic inflammatory penumbra after strokes. *Stroke* **44**, 1988–1996 (2013).
23. L. Park, K. G. Raman, K. J. Lee, Y. Lu, L. J. Ferran Jr., W. S. Chow, D. Stern, A. M. Schmidt, Suppression of accelerated diabetic atherosclerosis by the soluble receptor for advanced glycation endproducts. *Nat. Med.* **4**, 1025–1031 (1998).
24. H. Offner, S. Subramanian, S. M. Parker, C. Wang, M. E. Afentoulis, A. Lewis, A. A. Vandenbark, P. D. Hurn, Splenic atrophy in experimental stroke is accompanied by increased regulatory T cells and circulating macrophages. *J. Immunol.* **176**, 6523–6531 (2006).
25. A. Hug, A. Dalpke, N. Wieczorek, T. Giese, A. Lorenz, G. Auffarth, A. Liesz, R. Veltkamp, Infarct volume is a major determiner of post-stroke immune cell function and susceptibility to infection. *Stroke* **40**, 3226–3232 (2009).
26. B. G. Talayero, F. M. Sacks, The role of triglycerides in atherosclerosis. *Curr. Cardiol. Rep.* **13**, 544–552 (2011).
27. G. Courties, F. Herisson, H. B. Sager, T. Heidt, Y. Ye, Y. Wei, Y. Sun, N. Severe, P. Dutta, J. Scharff, D. T. Scadden, R. Weissleder, F. K. Swirski, M. A. Moskowitz, M. Nahrendorf, Ischemic stroke activates hematopoietic bone marrow stem cells. *Circ. Res.* **116**, 407–417 (2015).
28. M. Nahrendorf, M. J. Pittet, F. K. Swirski, Monocytes: Protagonists of infarct inflammation and repair after myocardial infarction. *Circulation* **121**, 2437–2445 (2010).
29. Y. Katayama, M. Battista, W.-M. Kao, A. Hidalgo, A. J. Peired, S. A. Thomas, P. S. Frenette, Signals from the sympathetic nervous system regulate hematopoietic stem cell egress from bone marrow. *Cell* **124**, 407–421 (2006).
30. Á. Chamorro, A. Meisel, A. M. Planas, X. Urra, D. van de Beek, R. Veltkamp, The immunology of acute stroke. *Nat. Rev. Neurol.* **8**, 401–410 (2012).
31. A. Liesz, H. Rüger, J. Purrucker, M. Zorn, A. Dalpke, M. Möhlenbruch, S. Englert, P. P. Nawroth, R. Veltkamp, Stress mediators and immune dysfunction in patients with acute cerebrovascular diseases. *PLOS ONE* **8**, e74839 (2013).
32. D. J. Antoine, H. E. Harris, U. Andersson, K. J. Tracey, M. E. Bianchi, A systematic nomenclature for the redox states of high mobility group box (HMGB) proteins. *Mol. Med.* **20**, 135–137 (2014).
33. E. Venereau, M. Casalgrandi, M. Schiraldi, D. J. Antoine, A. Cattaneo, F. De Marchis, J. Liu, A. Antonelli, A. Preti, L. Raeli, S. S. Shams, H. Yang, L. Varani, U. Andersson, K. J. Tracey, A. Bachi, M. Uguccioni, M. E. Bianchi, Mutually exclusive redox forms of HMGB1 promote cell recruitment or proinflammatory cytokine release. *J. Exp. Med.* **209**, 1519–1528 (2012).
34. L. Boring, J. Gosling, M. Cleary, I. F. Charo, Decreased lesion formation in CCR2$^{-/-}$ mice reveals a role for chemokines in the initiation of atherosclerosis. *Nature* **394**, 894–897 (1998).
35. J. Guo, M. Van Eck, J. Twisk, N. Maeda, G. M. Benson, P. H. E. Groot, T. J. C. Van Berkel, Transplantation of monocyte CC-chemokine receptor 2–deficient bone marrow into ApoE3–Leiden mice inhibits atherogenesis. *Arterioscler. Thromb. Vasc. Biol.* **23**, 447–453 (2003).
36. C. S. Robbins, I. Hilgendorf, G. F. Weber, I. Theurl, Y. Iwamoto, J.-L. Figueiredo, R. Gorbatov, G. K. Sukhova, L. M. S. Gerhardt, D. Smyth, C. C. J. Zavitz, E. A. Shikatani, M. Parsons, N. van Rooijen, H. Y. Lin, M. Husain, P. Libby, M. Nahrendorf, R. Weissleder, F. K. Swirski, Local proliferation dominates lesional macrophage accumulation in atherosclerosis. *Nat. Med.* **19**, 1166–1172 (2013).
37. B. Coll, C. Alonso-Villaverde, J. Joven, Monocyte chemoattractant protein-1 and atherosclerosis: Is there room for an additional biomarker? *Clin. Chim. Acta.* **383**, 21–29 (2007).

38. J. Cros, N. Cagnard, K. Woollard, N. Patey, S.-Y. Zhang, B. Senechal, A. Puel, S. K. Biswas, D. Moshous, C. Picard, J.-P. Jais, D. D'Cruz, J.-L. Casanova, C. Trouillet, F. Geissmann, Human CD14^{dim} monocytes patrol and sense nucleic acids and viruses via TLR7 and TLR8 receptors. *Immunity* **33**, 375–386 (2010).
39. C. Kilkenny, W. J. Browne, I. C. Cuthill, M. Emerson, D. G. Altman, Improving bioscience research reporting: The ARRIVE guidelines for reporting animal research. *PLOS Biol.* **8**, e1000412 (2010).
40. N. Saederup, A. E. Cardona, K. Croft, M. Mizutani, A. C. Cotleur, C.-L. Tsou, R. M. Ransohoff, I. F. Charo, Selective chemokine receptor usage by central nervous system myeloid cells in CCR2-red fluorescent protein knock-in mice. *PLOS ONE* **5**, e13693 (2010).
41. J. B. Bederson, L. H. Pitts, M. Tsuji, M. C. Nishimura, R. L. Davis, H. Bartkowski, Rat middle cerebral artery occlusion: Evaluation of the model and development of a neurologic examination. *Stroke* **17**, 472–476 (1986).
42. H. R. Lo, Y. C. Chao, Rapid titer determination of baculovirus by quantitative real-time polymerase chain reaction. *Biotechnol. Prog.* **20**, 354–360 (2004).
43. S. Qin, H. Wang, R. Yuan, H. Li, M. Ochani, K. Ochani, M. Rosas-Ballina, C. J. Czura, J. M. Huston, E. Miller, X. Lin, B. Sherry, A. Kumar, G. Larosa, W. Newman, K. J. Tracey, H. Yang, Role of HMGB1 in apoptosis-mediated sepsis lethality. *J. Exp. Med.* **203**, 1637–1642 (2006).
44. M. J. Butcher, M. Herre, K. Ley, E. Galkina, Flow cytometry analysis of immune cells within murine aortas. *J. Vis. Exp.* **53**, 2848 (2011).
45. E. Maganto-Garcia, M. Tarrio, A. H. Lichtman, Mouse models of atherosclerosis. *Curr. Protoc. Immunol.* **Chapter 15**, 11–23 (2012).
46. T. A. Seimon, Y. Wang, S. Han, T. Senokuchi, D. M. Schrijvers, G. Kuriakose, A. R. Tall, I. A. Tabas, Macrophage deficiency of p38α MAPK promotes apoptosis and plaque necrosis in advanced atherosclerotic lesions in mice. *J. Clin. Invest.* **119**, 886–898 (2009).
47. D. J. Antoine, D. P. Williams, A. Kipar, R. E. Jenkins, S. L. Regan, J. G. Sathish, N. R. Kitteringham, B. K. Park, High-mobility group box-1 protein and keratin-18, circulating serum proteins informative of acetaminophen-induced necrosis and apoptosis in vivo. *Toxicol. Sci.* **112**, 521–531 (2009).
48. S. Nyström, D. J. Antoine, P. Lundbäck, J. G. Lock, A. F. Nita, K. Högstrand, A. Grandien, H. Erlandsson-Harris, U. Andersson, S. E. Applequist, TLR activation regulates damage-associated molecular pattern isoforms released during pyroptosis. *EMBO J.* **32**, 86–99 (2013).
49. X. Ge, D. J. Antoine, Y. Lu, E. Arriazu, T.-M. Leung, A. L. Klepper, A. D. Branch, M. I. Fiel, N. Nieto, High mobility group box-1 (HMGB1) participates in the pathogenesis of alcoholic liver disease (ALD). *J. Biol. Chem.* **289**, 22672–22691 (2014).

Acknowledgments: We thank K. Thuß-Silczak for excellent technical assistance and U. Deutsch for maintaining transgenic mouse colonies at the University of Bern. CCR2$^{RFP/RFP}$CX3CR1$^{GFP/+}$ mice were donated by I. F. Charo (University of California, San Francisco, USA) and R. Ransohoff (Biogen Idec, Boston, USA). sRAGE baculovirus was a donation by A.-M. Schmidt (New York University Langone Medical Center, New York City, USA). **Funding:** This study was funded by the excellence cluster of the German research foundation Munich Cluster for Systems Neurology (SyNergy) (EXC1010 to M.D., A.L., and J.B.) and the German Research Foundation (DFG) (LI-2534/2-1 to A.L., SFB1123-A03 to J.B., and SFB1123-B01 to L.M.H.). **Author contributions:** S.R. performed most of the experiments, analyzed the data, and wrote the manuscript. V.S. performed the fluorescence-activated cell sorting experiments and monocyte stimulation assays. S.T. acquired and analyzed the patient cohort. L.S. performed the MAEC stimulation experiments. G.H. and A.G. produced sRAGE. D.J.A. performed and analyzed the HMGB1 mass spectrometry. A.A., C.O., M.G., A.F., and D.V. performed in vivo MRI experiments and analyzed the imaging data. L.M.H. performed the blood biochemistry. D.V., H.E.H., B.E., and M.E.B. contributed the critical material and techniques for this study. C.H., J.B., and M.D. contributed the critical input to study design and manuscript writing. A.L. initiated and coordinated the study, analyzed the data, and wrote the manuscript. **Competing interests:** The authors declare that they have no competing interests. **Data and materials availability:** All primary data, detailed protocols, and noncommercially available materials can be requested from the corresponding author. The sRAGE vector was obtained under a material transfer agreement from A.-M. Schmidt (New York University School of Medicine, New York City, NY, USA).

Submitted 16 June 2017
Accepted 14 February 2018
Published 14 March 2018
10.1126/scitranslmed.aao1313

Citation: S. Roth, V. Singh, S. Tiedt, L. Schindler, G. Huber, A. Geerlof, D. J. Antoine, A. Anfray, C. Orset, M. Gauberti, A. Fournier, L. M. Holdt, H. E. Harris, B. Engelhardt, M. E. Bianchi, D. Vivien, C. Haffner, J. Bernhagen, M. Dichgans, A. Liesz, Brain-released alarmins and stress response synergize in accelerating atherosclerosis progression after stroke. *Sci. Transl. Med.* **10**, eaao1313 (2018).

Science Translational Medicine

Brain-released alarmins and stress response synergize in accelerating atherosclerosis progression after stroke

Stefan Roth, Vikramjeet Singh, Steffen Tiedt, Lisa Schindler, Georg Huber, Arie Geerlof, Daniel J. Antoine, Antoine Anfray, Cyrille Orset, Maxime Gauberti, Antoine Fournier, Lesca M. Holdt, Helena Erlandsson Harris, Britta Engelhardt, Marco E. Bianchi, Denis Vivien, Christof Haffner, Jürgen Bernhagen, Martin Dichgans and Arthur Liesz

Sci Transl Med **10**, eaao1313.
DOI: 10.1126/scitranslmed.aao1313

An alarmin(g) consequence of stroke

Patients surviving a stroke are at an increased risk for subsequent cardiovascular events. Preclinical models have shown accelerated atherosclerosis after stroke; however, the mechanisms underlying this enhanced plaque formation and inflammation in arteries have not been investigated. Now, Roth *et al*. have discovered that stroke-induced alarmin high-mobility group box 1 (HMGB1) release and sympathetic stress response activation exert a synergistic effect, resulting in exacerbation of atherosclerotic plaques in mice. The authors suggest that interfering with these processes after stroke might reduce the risk of secondary cardiovascular events.